POLARIMETRIC MEASUREMENTS OF SEA SURFACE BRIGHTNESS TEMPERATURES USING AN AIRCRAFT K-BAND RADIOMETER

Simon H. Yueh, William J. Wilson, Son V. Nghiem, Fuk K. Li and William B. Ricketts

Jet Propulsion Laboratory
California Institute of Technology
4800 Oak Grove Drive
Pasadena, CA 91109
Tel: (818) 354-3012, Fax: (818) 393-5285

Submitted to IEEE Trans. Geosci. Remote Sensing

February 7, 1994

Abstract

This paper presents the first experimental evidence that the polarimctric brightness temperatures of sea surfaces arc sensitive to ocean wind direction in the incidence angle range of 30 to 50 degrees. Our experimental data were collected by *a* K-band (19.35 GHz) polarimctric radiometer (WINDRAD) mounted on the NASA DC-8 aircraft. A set of aircraft radiometer flights was successfully completed in November 1993. Wc performed circle flights over NDBC moored buoys deployed off the northern California, coast, which provided ocean wind measurements. The first WI NDRAD flight was made on November 4, 1993. '1'here was clear weather with a wind speed of 12 m/s at 330 degrees around the Pt. Arena buoy. Wc circled the buoy at three incidence angles, and all data when plotted as functions of azimuth angles show clear modulations of several degrees Kelvin. At 40 degrees incidence angle, there is a 5 degrees Kelvin peak-to-peak signal in the second Stokes parameter Q and the third Stokes parameter U. The Q data maximum is in the upwind direction and U has a 45 degrees phase shift in azimuth - as predicted by theory. There is also an up/downwind asymmetry of 2 degrees Kelvin in the Q data, and 1 degree Kelvin in the U data. At 50 degrees incidence angle, the collected data show very similar wind direction signatures to the SSM/I model function. Additional flights were made on other days under cloudy conditions. Data taken at a wind speed of 8 m/s show that at 40 degrees incidence Q and U have a smaller azimuthal modulation of 3 degrees Kelvin, probably due to the lower wind speed. Additionally, the simultaneously rccordcd video images of sea surfaces suggested that Q and U data were less sensitive to clouds, breaking waves and whitecaps, while the T_v and T_h increased by a few degrees Kelvin when the radiometer beam crossed over clouds, or there was a sudden increase of whitecaps in the radiometer footprint. The results of our aircraft frights clearly indicate that passive polarimctric radiometry is a viable option in space remote sensing of ocean surface wind direction as well as wind speed.

1 Introduction

Global measurements of near surface ocean wind are crucial for many oceanographic and atmospheric studies. The near surface wind generates the momentum flux affecting ocean circulation and mixing and is the kcy driving force in air-sea interaction processes. A potential sensor for ocean wind remote sensing is the passive microwave radiometer. Examples of such radiometers include the Scanning Multichannel Microwave Radiometer (SMMR) flown on NIMBUS-7 and SEASAT and the Special Sensor Microwave/Imager (SSM/I) deployed on the DMSP missions [1]. Passive radiometers measure the thermal emission from sca surfaces, which is affected by surface roughness, temperature, foam, salinity, atmospheric water content and other factors. Although it is commonly accepted that microwave radiometers can measure ocean wind speeds based on the sensitivity of thermal emission on surface roughness, it was not clear whether passive microwave radiometer measurements were sensitive to wind direction until the recent experimental observations [2, 3, 4] indicated that ocean thermal radiation could vary over azimuthal angles relative to the wind by a few degrees Kelvin.

Etkin et al. [2] measured the azimuthal dependence of brightness temperatures of vertical and horizontal polarizations (T_v and T_h) using their aircraft radiometers at near grazing (incidence angle of 78°) at 20 GHz and at normal incidence at 3.7, 20, and 37 GHz. Their results showed that the azimuthal modulation dropped rapidly with increasing electromagnetic wavelength. Unfortunately, the measurements they reported did not include the range of incidence angle traditionally used by spaceborne microwave radiometers (incidence angles of about 48° to 60°) for large swath coverage.

In contrast, the SSM/I measures the brightness temperatures at an incidence angle of 53 degrees. Wentz [3] collocated the SSM/I data. with the buoy-measured wind vector and found that T_h and T_v at both 19 and 37 GHz could vary with the wind direction by a few degrees Kelvin. Based on this wind direction signal, he further produced a monthly mean ocean wind map using the SSM/I data, demonstrating the applicability of passive radiometer

technique to global ocean wind measurements from space.

While conventional radiometers measure the brightness temperatures with vertical and horizontal polarizations, the results from Dzura et al. [4] suggest that radiometric signatures at other polarization states arc also sensitive to wind direction. In fact, the full polarization state of thermal emission from water surfaces can be characterized by four Stokes parameters I, Q, U, and V, which are related to the horizontal and vertical polarization components of the radiated electric fields illustrated in Figure 1. Ground-based microwave radiometer measurements of water surfaces with artificially constructed directional features [5, 6] have shown that, in addition to I and Q, the third Stokes parameter U also had azimuthal variations. Nevertheless, although these ground-based studies provided valuable physical insight into the mechanisms responsible for the azimuth modulation signatures, the approximately sinusoidal surface profiles were too simplistic compared with sea surfaces.

The experimental results presented by Dzura et al. [4] were data collected by an aircraft Ku-band radiometer at normal incidence (incidence angle of O degrees). Figure 5 in their paper showed that when the second Stokes parameter reached maximum, the third Stokes parameter was nearly zero, and vice versa, The observed azimuthal variations of the second and third Stokes parameters have been shown to agree qualitatively with the predictions of a two-scale surface emission model analysis [8]. However, since only one example was reported and the data were collected at normal incidence, which is not so appropriate for space remote sensing if a large swath coverage is requi red, more extensive obscrvat ions of the azimuthal variations of Stokes parameters over wind speeds and incidence angles arc required to evaluate the applicability of polarimetric radiometry to ocean surface winds.

Theoretical studies of polarimetric emission in the middle range of incidence angles have been carried out by Yueh et al. [8] using a two-scale sea surface model with the small scale surface scattering modelled by Bragg scattering [7]. Their results were in reasonable agreement with the data reported by Etkin et al. [2] and the SSM/I data. Additionally, it was found that the U parameter was an odd function with respect to the wind direction

with its peaks occurring at approximately 45 degrees away from the wind direction, and its azimuth modulation magnitudes were comparable to that of Q parameter. Their study suggested that because of the relative azimuth phase shift between Q and *U*, it would be possible to achieve good wind vector measurements across all parts of swath using a spaceborne polarimetric radiometer. Although their theoretical results indicated promising applications, no experimental data collected in the incidence angle range of 30 to 60 degrees were yet available.

To explore the potential of the polarimetric radiometry technique for further space remote sensing consideration, we built a K-band multi-polarization radiometer deployed on the NASA I) C-8 aircraft with circle flights over several ocean buoys to study sea surface emissions. Section 2 describes the designs of our K-band (19.35 GHz) microwave radiometer and our first set of aircraft experiments, and details the data reduction methods. 'l'he measured brightness temperature data are presented in Section 3 in terms of their correlation with wind direction. Section 4 summarizes the results of this paper.

2 Multi-polarization Microwave Radiometer Measurements And Data Calibration

To measure all four Stokes parameters, a K-band microwave! multi-polarization radiometer (WINDRAD) for ocean wind remote sensing was completed in October 1993. This radiometer is a direct detection Dicke-switch radiometer with noise injection to achieve better balance between the alternating antenna and reference measurements. ('l'he noise source was on when taking ocean measurements and off when the Dicke switch was switched to reference load,) All microwave components are mounted on a temperature-controlled plate to achieve good gain stability and are in a metallic box for thermal insulation and to prevent external microwave interference.

The WI NDRAD block diagram is shown in Figure 2 and its key parameters are shown in Table 1. The electric fields entering the antenna are split into horizontal and vertical

polarization components (E_h and E_v) by an orthogonal mode transducer (OMT). A microwave waveguide switch network (Figure 2) is then used to produce four polarizations using these two linearly polarized orthogonal components. In the waveguide switch network, a Magic-Tee is used to take the sum and the difference of vertically and horizontally polarized electric fields to produce the 45 and -45 linear polarizations with the phase shifter set at the O-degree-phase position, If the phase shifter is set at the 90 degrees phase shift position by a manual switch, these two 45 and -45 linear polarizations become left- and right-hand circular polarizations. These four polarizations were scanned sequentially with the switch 'positions commanded by a persona] computer, which allows us to repeatedly measure three Stokes parameters and record the data automatically. Throughout our experiments, wc did not usc the 90-degree phase shift option because of limited available flight hours, and hence only the first three Stokes parameters were measured.

The radiometric calibration converting the radiometer voltage outputs into brightness temperatures was performed using the radiometer parameters measured in the laboratory and the ancillary thermistor measurements taken during the aircraft flights. To measure the noise diode temperature in the laboratory, wc replaced the reference load by a small K-band horn (about 2 inches long), switched the Dicke switch to the small horn, and took the hot load (absorber) measurements with the noise diode switch on and off and the cold load (liquid nitrogen) measurements with the noise diode switch off. These measurements allowed us to calculate the noise diode temperature, which subsequently enabled us to calculate the losses for all polarization channels from the antenna used for flight experiments to the Dicke switch using the hot/cold load calibration technique. During circle flights, the physical temperatures of the waveguide switch network, the reference load, the OMT, and the antenna. horn were measured by using the thermistors attached on these components and recorded by the personal computer about once pcr minute allowing us to detect any sensible temperature changes. These losses and temperature measurements gave us the slope and the zero-intercept of the straight line for voltage to brightness temperature conversion. Wc

examined the absolute accuracy of the conversion formula for each polarization channel by comparing the brightness temperatures of hot and cold loads against the temperature of the absorber measured by a thermistor and the liquid nitrogen temperature (77 K), and we found that the differences were less than 2 K for all polarization channels.

After its completion, the WINDRAD was mounted in the window of the NASA DC-8 aircraft. A set of radiometer flights over ocean surfaces were performed in November 1993 to measure polarimetric brightness temperatures of sea surface under a variety of wind/atmospheric conditions. We performed circle flights over selected NDBC moored buoys deployed off the coast of the northern California, which provided ocean wind speed and direction data in addition to other associated oceanic measurements. With the antenna fix-mounted on the DC-8 at an incidence angle of 60 degrees when the DC-8 flies level, the DC-8 was banked at several different roll angles to allow us to observe the ocean at various incidence angles.

in addition to radiometer data and NDBC buoy data, aircraft navigation data transmitted through the I) C-$ DADS serial bus were also recorded by the personal computer. The DC-8 DADS housekeeping data include the DC-8 pitch, roll and heading angles, ground speed, altitude, and etc.. It was found that the DC-8 roll and pitch angles would typically change gradually by a few degrees during the circle flights. The main effect of the pitch angle drift is to cause an angular offest between the polarization basis vectors parallel to the antenna vertical and horizontal polarization channels and those with respect the water surface. However, with the knowledge of aircraft pitch and roll angles, we used the coordinate transformation between these two polarization coordinate systems to derive the relative alignment angle (χ) between these two sets of polarization vectors in addition to the incidence angle (θ) with respect to the water surface. Using the relative alignment angle, we then converted the Stokes parameters measured relative to the antenna coordinate into these with respect to water surface coordinate using the following transformation:

$$I = I_a \tag{1}$$

$$Q = Q_a \cos 2\chi + U_a \sin 2\chi \quad (2)$$

$$U = U_a \cos 2\chi - Q_a \sin 2\chi \quad (3)$$

$$v = V_a \quad (4)$$

where the subscript 'a' indicates these quantities measured with respect to the antenna coordinate system, while quantities without subscript arc defined in the water surface coordinate system.

Besides its effect on the polarization basis alignment, the aircraft attitude variation can also cause an incidence angle drift. 'l'he actual incidence angle was affected most significantly by the aircraft roll angle variation during circle flights. Because the incidence angle variations were expected to cause significant changes in the T_v and T_h brightness temperatures, wc took additional brightness temperatures over a wide range of incidence angles from 30 to 80 degrees by wing-wagging the aircraft. Figure 3 illustrates the measured brightness temperature data as a function of incidence angle and the corresponding third-order polynomial fits. Our approach for the incidence angle effect correction was to first calculate the average incidence angle over a full set of circles and then calculate the difference between the instantaneous incidence angle and the average angle. The difference is converted into an expcctcd brightness temperatures variation using the empirical t}lird-order polynomials, which is then used to translate the measured T_v and T_h data into those that would be measured as if the incidence angle had remained constant at the average incidence angle. After we inspected the T_v, T_h, and Q data measured with multiple continuous circles, the data after correction were nearly symmetric with respect to the wind direction and more repeatable over the sequence of circles, indicating that the above-mentioned empirical correction technique performed reasonabl y well. Although this empirical approach appeared reasonable, we recognize that it could only provide a first-order correction and some errors remain uncompensated, since brightness temperatures are expected to be functions of other other environmental variables like cloud water and may not be correctly modelled by polynomials with fixed coefficients.

Note that similar incidence angle correction was not carried out for the U data, since

it seemed that U was a relatively weak function of incidence angle according to the data collected from 30 to 50 degrees incidence showing that U apparently varied by less than 1 K over a change of 20 degrees incidence angle. Hence no incidence angle correction was deemed necessary.

Our third Stokes parameter U data is in fact derived from the 45 and -45-degrees polarization brightness temperatures denoted by T_p and T_m (see Figure 1). If there is cross-coupling between the antenna horizontal and vertical channels, and if the losses between these two polarization channels leading from the OMT to the Magic-Tee outputs are not perfectly compensated by calibration, the resulting U measurements will have bias terms. This error term can be shown to have the following form, if a linear system is assumed for our radiometer:

$$\mathrm{AU} = c_1 T_v + c_2 T_h + \mathrm{C}_3 \tag{5}$$

We estimated these three coefficients using the data itself based on the fact that the average value of U over a complete circle should be zero because U should be an odd function with respect to the wind direction. For each set of circle flight, we averaged the values of U, T_v, and T_h over a complete circle. Using all circle flights data, we performed a linear-regression of the U-average data (not zero) with the T_v and T_h data. The resulting estimation was $c_1 = 0.0194$, $c_2 = -0.00926$, and $c_3 = -2.634$, and the rms difference between the U-bias term estimated using the linear-regression curve and the measured U-average data was 0.22. The bias correction formula was used to correct the U data using the coincidental T_v and T_h measurements. We found that the I) C-bias terms seen in the original U data were effectively removed, while there was no noticeable change in the shape of U data with respect to the azimuth angle.

3 Azimuth Signatures of Measured Stokes parameters

To study the azimuthal modulations of brightness temperatures, we correlated the multi-polarization measurements with the azimuth angle ϕ, the angle between the wind direction

(ϕ_w) and the radiometer azimuth look angle (ϕ_r), i.e.,@== ϕ_w -4,. With this definition, ϕ = 0 (180) degrees corresponds to the upwind (downwind) direction, Because the NDBC buoys provide wind speed and direction measurements only once per our, the buoy data collected at the time closest to the time of each circle flight is used. 'l'his is not expected to cause significant error because for our flights, wc found that the buoy measured wind before and after the circle flights changed by less than or equal to 10 degrees in direction and less than 2 knots in speed. Hence, no interpolation was performed to estimate the wind speed and direction at the exact time of flight.

Figure 4 illustrates the measured Stokes parameters, collected at 30 degrees incidence, as functions of azimuth angle ϕ. I'here are clear azimuth modulations in all measured Stokes parameters with an approximate 3 K peak-to-peak signal in T_v and T_h and a 5 K signal in Q and U data, The peaks of T_v occur at up/downwind direction, and the minima at crosswind direction, while T_h peaks at crosswind direction and reaches minimum at up/downwind direction. These modulation signatures agree with the data collected at normal incidence by Dzura et al. [4] and Etkin et al. [2], the SSM/I model function [3], ground-based measurements [5, 6] and the theoretical predictions by Yueh et al. [7, 8]. However, unlike the normal incidence measurements and the ground-based experiments using symmetric surfaces, there are up/downwind asymmetry (brightness difference between the up and downwind direction measurements) of about 1.3, 0.2, and 1.1 K in T_v, T_h, and Q, respectively, in our aircraft data. This up/downwind asymmetry could be caused by the hydrodynamic modulation of the capillary waves, or could be explained by the observations that the whitecaps in the downwind side arc brighter than those in the upwind side [9]. In addition, it can be noticed that along the wind direction, U is close to (should be according to reflection symmetry) zero and reaches maximum at about 45 degrees away from the wind direction. Furthermore, unlike T_v, T_h, and Q data, U is an odd function of azimuth angle with respect to the wind direction. The relative azimuth phase shift between U and Q data may lead to good wind measurement performance across all parts of swath as discussed by

Yueh et al. [7].

Taking a closer look at Figure 4, we noticed that T_v and T_h curves had a few spikes located at several azimuth angles, and were not as smooth as Q and U data. For example, T_h did not reach the expected minimum at $\phi = 900$ degrees (downwind direction), smeared with some noise. After we visually reviewed the video tape recorded at the same time with the brightness measurements, it appeared that at these few moments, there were isolated, sudden increases of wave breakings and sustained whitecaps in the radiometer footprint. Therefore it would not be surprising to find simultaneous brightness temperature increases of 1 to 2 K in all radiometer channels [9]. However, these additional signals were apparently unpolarized, and hence, did not introduce corresponding effects in the Q and U data. This suggests that Q and U are less susceptible to such unpolarized geophysical variations.

Figure 5 plots the data collected at 40 degrees incidence angle, The azimuth signatures of all measured Stokes parameters as well as the peak-to-peak signals are similar to those taken at 30 degrees incidence, indicating that the wind direction signals are smooth function of incidence angle from 30 to 40 degrees. Again the spikes in the T_v and T_h data around the azimuth angle of 180 degrees are found at times with enhanced breaking waves and whitecaps.

Besides the data mentioned above, one circle flight was also performed for the incidence angle of about 50 degrees with an average value of 49 degrees, and the Stokes parameter data are illustrated in Figure 6. To allow easy comparison with the SSM/I wind direction signal, the SSM/I model function at the measured wind speed are also included. To place the SSM/I data together with our data, we added constant offsets of 4 and 25.5 to the SSM/I T_v and T_h data, respectively, which were possibly due to the atmospheric radiation, not removed from our measurements unlike the SSM/I data, and the difference in incidence angles (49 degrees for our data against 53 degrees for the SSM/I). The difference between these two offsets could be due to that the sea surfaces are better reflectors for horizontal polarization than vertical polarization, hence, reflecting more horizontally polarized downwelling atmospheric

radiation than vertically polarized radiation into the receiver, and could also be caused by the incidence angle, difference of 4 degrees, resulting in different sea surface emissivities at these two incidence angles with an expected enhancement in T_h offset, while a reduction in T_v offset according to the incidence angle effects illustrated in Figure 3. Nevertheless, the azimuth modulation signatures of our T_v and T_h data show very close resemblance to the SSM/1 data collected at 53 degrees incidence, and in particular the vertical polarization brightness T_v did not have an obvious peak in the downwind direction like the SSM/I model. The absence of brightness peak in the downwind direction in the T_v data results in the observed, relatively small second harmonic coefficient.

A typical form of geophysical model functions, relating the thermal radiation signatures to the geophysical surface parameters, expresses the Stokes parameters in the Fourier series of the azimuth angle ϕ. For wind-generated sea surfaces, it is expected that the surfaces are statistically reflection symmetric with respect to the wind direction represented by ϕ = O. Using reflection symmetry, it can be shown that I and Q (or T_v and T_h) are even functions of ϕ, whereas U and V arc odd functions. Hence, expanded only to the second harmonic of ϕ,

$$I \simeq I_0 + I_1 \cos\phi + I_2 \ \text{Cos} \ 2\phi \tag{6}$$

$$Q \simeq Q_0 + Q_1 \cos\phi + Q_2 \cos 2\phi \tag{7}$$

$$U \simeq U_1 \sin\phi + U_2 \sin 2\phi \tag{8}$$

$$V \simeq V_1 \sin\phi + V_2 \sin 2\phi \tag{9}$$

Like I and Q, T_v and T_h arc expanded by the cosine series.

We extracted the harmonic coefficients from the data presented in Figures 4 to 6 and included the second harmonic approximation curves in Figures 4 and 5 for comparison. We found that the second harmonic expansion appeared to be a good approximation, in particular for the Q and U parameters.

Figure 7 illustrates the incidence angle dependence of the harmonic coefficients. The first

harmonic coefficients of all Stokes parameters have a rising trend with increasing incidence angles, meaning that the up/downwind asymmetry is larger at a higher incidence angle. The first harmonic of T_v is about 3 times of that of T_h, indicating that vertical polarization is more strongly affected by the up/downwind asymmetric features of sca surfaces than horizontal polarization. Unlike the first harmonics, all the second harmonics have a slow decreasing trend as the incidence angle increases. The second harmonic modulation amplitudes of Q and U arc about 2 times of that of T_v or T_h. That is, even though the radiometer signal sensitivity of Q and U, which arc calculated as the difference between two polarization measurements, is typically $\sqrt{2}$ times of that of T_v or T_h, their increased sensitivity to wind direction will more than offset the lower SNR. It is interesting to notice that the harmonic coefficients of Q are close to that of U, consistent with the theoretical predictions by Yueh et al. [7, 8].

The effects of clouds on the brightness temperature measurements are illustrated in Figurc 8. 'l'he data were taken at the incidence angle of about 40 degrees similar to the data plotted in Figure 5, and at the time of flight, right after a cold front with thick rain clouds passed over the buoy outside of the northern California. coast, there were many puffy clouds scattered in the sky. It was found that whenever the radiometer beam crossed the clouds, as expected, the brightness temperatures in all polarization channels would increase simultaneously by a few K, overwhelming the wind direction signals in T_v and T_h. In contrast, the Q and U data, which are expected to be insensitive to unpolarized radiations, are less affected by the clouds, displaying very similar azimuth signatures to the data taken under clear sky conditions shown in Figures 4 to 6. This indicates that polarimetric brightness measurements are useful even under cloudy conditions.

Again comparing Figure 5 with Figure 8 shows that the peak-to-peak signals in the Q and U data in Figure 5 are about 3 K, less than the 5 K signal shown in Figure 5. 'I'his is probably related to the reduction of wind speed, about 8 m/s for the data presented in Figure 8 compared with 12 m/s for Figure 5.

4 Summary

We have completed a set of proof-of-concept aircraft measurements of the K-band multi-polarization brightness temperatures of sea surfaces, detecting a few degrees K dependence on wind direction. The WINDRAD data show that T_v, T_h and Q are even functions of the wind direction, while the third Stokes parameter U is an odd function - as predicted by a two-scale surface scattering mode] [8]. in addition, the data collected at 50 degrees incidence angle arc very similar to the SSM/I brightness temperature data, particularly, the absence of vertical polarization peak in the downwind direction in both data sets. Comparing Q and U data curves with T_v and T_h curves indicates that Q and U data arc less sensitive to clouds, breaking waves and whitecaps, which arc strong thermal radiation sources. This suggests that Q and U are potentially better indicators for wind direction measurements. In conclusion, our aircraft radiometer flights show that the first three Stokes parameters of the thermal radiation from sea. surfaces have a sinusoidal variations relative to the wind direction from 30 to 50 degrees incidence with an amplitude of a few K, indicating that passive microwave radiometry is a viable option for global ocean wind vector measurements.

We recognize that because of limited flight hours and the oceanic/atmospheric conditions encountered, it is not possible to develop a comprehensive geophysical model function using our existing data set to examine more quantitatively the sensitivities on wind speeds, incidence angles and other atmospheric and ocean variables. Hence, more extensive aircraft measurements are planned to further our understanding of the multi-polarization brightness temperature signatures of sea surfaces.

5 Acknowledgment

This work was performed under contract with the National Aeronautics and Space Administration at the Jet Propulsion Laboratory, California Institute of Technology. The authors would like to thank the NASA Ames Research Center for assistance in aircraft flight experiments.

References

[1] Hollinger, J. P., J. L. Peirce, and G. A. Poe, "SSM/I Instrument Evaluation," *IEEE Trans. Geosci. Remote Sensing,* Vol. 28, No. 5, 781-790, Sept, 1990.

[2] Etkin, V. S., M.D. Raev, M.G. Bulatov, Yu.A. Militsky, A.V. Smirnov, V.Yu. Raizer, Yu.A. Trokhimovsky, V.G. Irisov, A.V. Kuzmin, K.Ts. Litovchenko, E.A. Bespalova, E.I. Skvortsov, M .N. Pospelov, and A.]. Smirnov, *Radiohydrophysical Aerospace Research of Ocean,* Report Hp-1749, Academy of Sciences, Space Research Institute, Moscow, USSR, 1991,

[3] Wentz, F. J., "Measurement of oceanic wind vector using satellite microwave radiometers," *IEEE Trans. Geosci. Remote Sensing,* Vol. 30, No. 5, 960-972, Sep., 1992,

[4] Dzura, M. S., V. S. Etkin, A. S. Khrupin, M. N. Pospelov, and M. D. Raev, "Radiometers-Polarimeters: principles of design and applications for sea surface microwave emission polarimetry," International Geoscience and Remote Sensing Symposium, Houston, 1992.

[5] Johnson, J. T., J. A. Kong, R. T. Shin, 1). H. Staelin, K. O'Neill and A. W. Lohanick, "Third stokes parameter emission from a periodic water surface," *IEEE* Trans. *Geosci. Remote Sensing,* Vol. 31, No. 5, 1066-1080, September 1993.

[G] Yueh, S. H., S. V. Nghiem, R. Kwok, W. J. Wilson, F. K. Li, J. T. Johnson, and J. A. Kong, "Polarimetric thermal emission from periodic water surfaces," *Radio Science,* January-February, 1994.

[7] Yueh, S. }1., R. Kwok, F. K. Li, S. V. Nghiem, W, J. Wilson, and J. A. Kong, "Polarimetric passive remote sensing of ocean wind vector," submitted for publication in *Radio Science,* April 1993,

[8] Yueh, S. H., R. Kwok, F. K. Li, S. V. Nghiem, W, J. Wilson, and J, A. Kong, "Polarimetric passive remote sensing of wind-generated sea surfaces and ocean wind vectors," Proceedings of Ocean symposium, Vol. 1, 31-36, Victoria, British Columbia, Canada, October 1993.

[9] Smith, P. M., "The emissivity of sea foam at 19 and 37 GHz," *IEEE Trans. Geosci. and Remote Sensing,* Vol. GE-26, 541-547, 1988.

List of Tables

~'able 1: WINDRAI) key parameters.

Parameter	Value
Frequency (GHz)	19.35
Antenna Beamwidth (degree)	3.6
Antenna Sidelobes (dB)	<-30
Polarization	*v, H,* 45(1.*),-45(W)
Dicke Switch Rate (Hz)	*500*
System Noise Temperature -I Background (K)	530
Radiometer Bandwidth (MHz)	*500*
RMS Noise Per Footprint (K)	0.06

*: Phase shifter set at 90 degrees phase shift

List of Figures

6 Measured Stokes parameters at 50 degrees incidence verus azimuth angle indicated by solid curves. Buoy closest to the circle reported 23 knots at 5 m elevation, which can be translated into 12 m/s at 20 m elevation, I)a.shed curve represents the SSM/I model function. . , . . , . . . , ... , . . 25

7 Harmonic coefficients of Stokes parameters plotted as functions of incidence angle, Buoy closest to the circle reported 23 knots at 5 m elevation, which can be translated into 12 m/s at 20 m elevation. 26

8 Measured Stokes parameters at 40 degrees incidence verus azimuth angle indicated by solid curves. The sky was partially cloudy with scattered puffy clouds. Buoy closest to the circle reported 14 knots at 5 m elevation, which can be translated into 8 m/s at 20 m elevation. Dashed curves represent the second harmonic approximation, ... *27*

$$\text{Stokes Vector} = \begin{vmatrix} I \\ Q \\ U \\ V \end{vmatrix} = \begin{bmatrix} T_v + T_h \\ T_v - T_h \\ T_p - T_m \\ T_l - T_r \end{bmatrix} = c \begin{bmatrix} \langle E_h E_h^* \rangle + \langle E_v E_v^* \rangle \\ \langle E_v E_v^* \rangle - \langle E_h E_h^* \rangle \\ 2\,\mathrm{Re} \langle E_v E_h^* \rangle \\ 2\,\mathrm{Im} \langle E_v E_h^* \rangle \end{bmatrix}$$

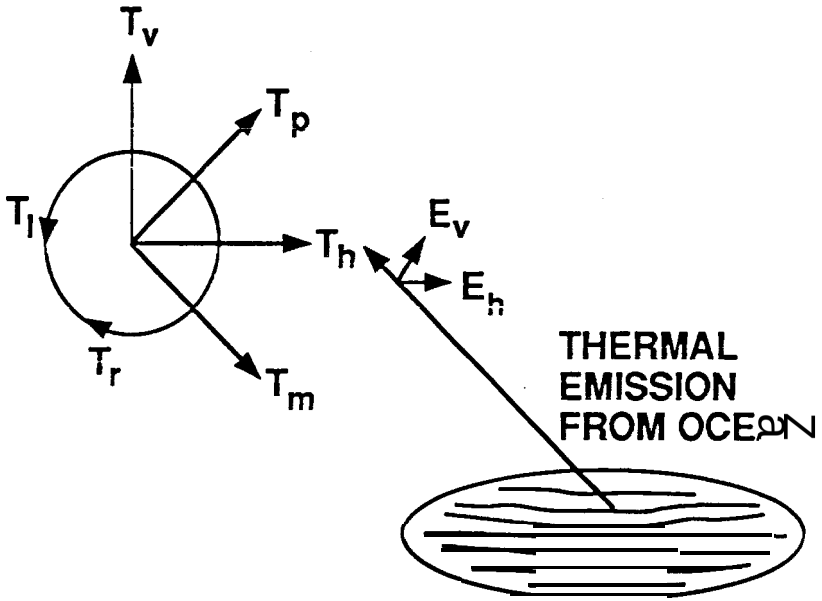

T_h : HORIZONTAL POLARIZATION

T_v : VERTICAL POLARIZATION

T_p : 45-degree POLARIZATION

T_m: -45-degree POLARIZATION

T_l : LEFT-HAND CIRCULAR POLARIZATION

T_r : RIGHT-HAND CIRCULAR POLARIZATION

Figure

Figure 2 19 GHz Wind Radiometer

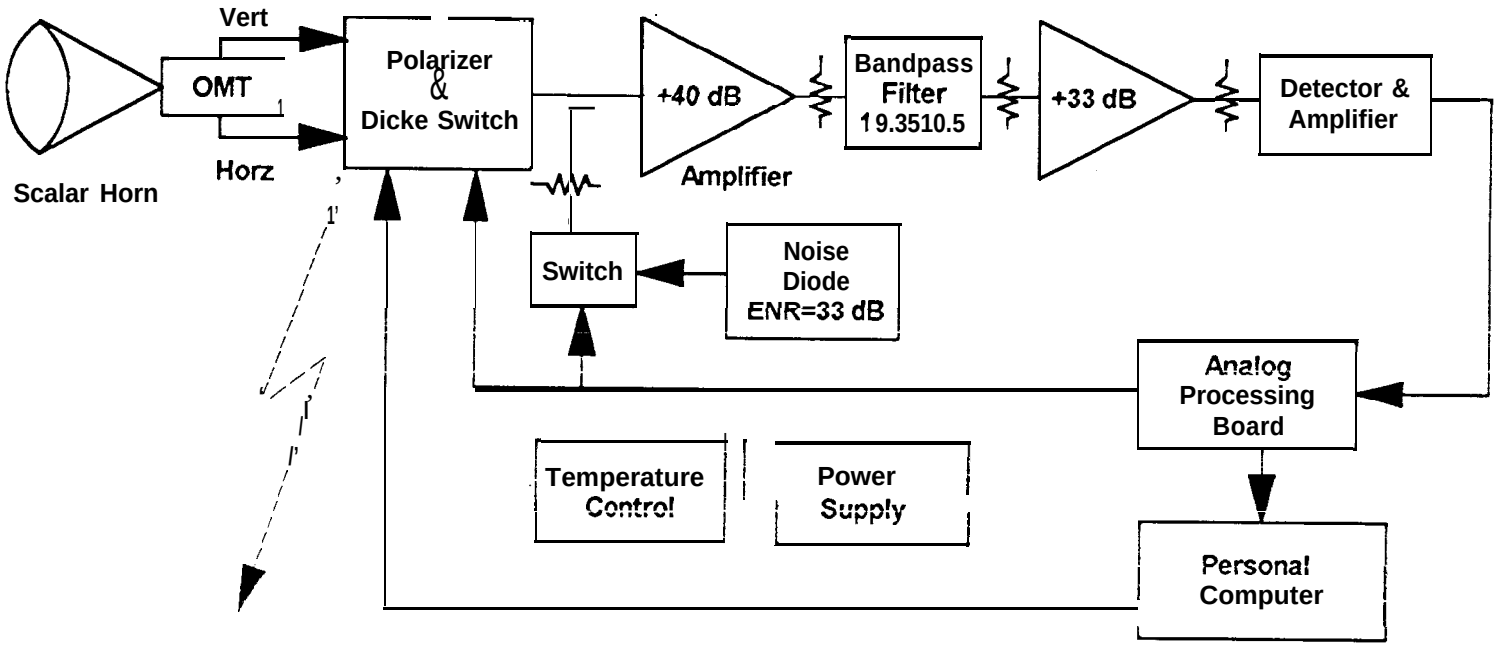

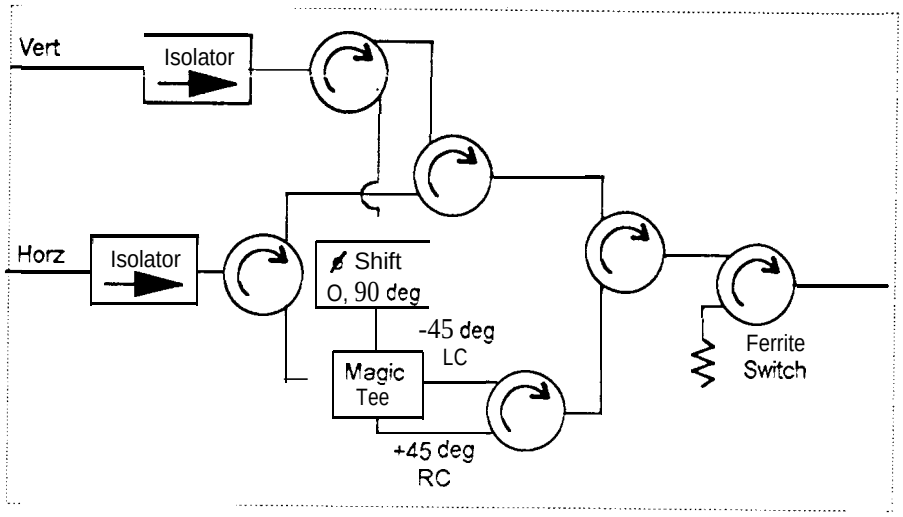

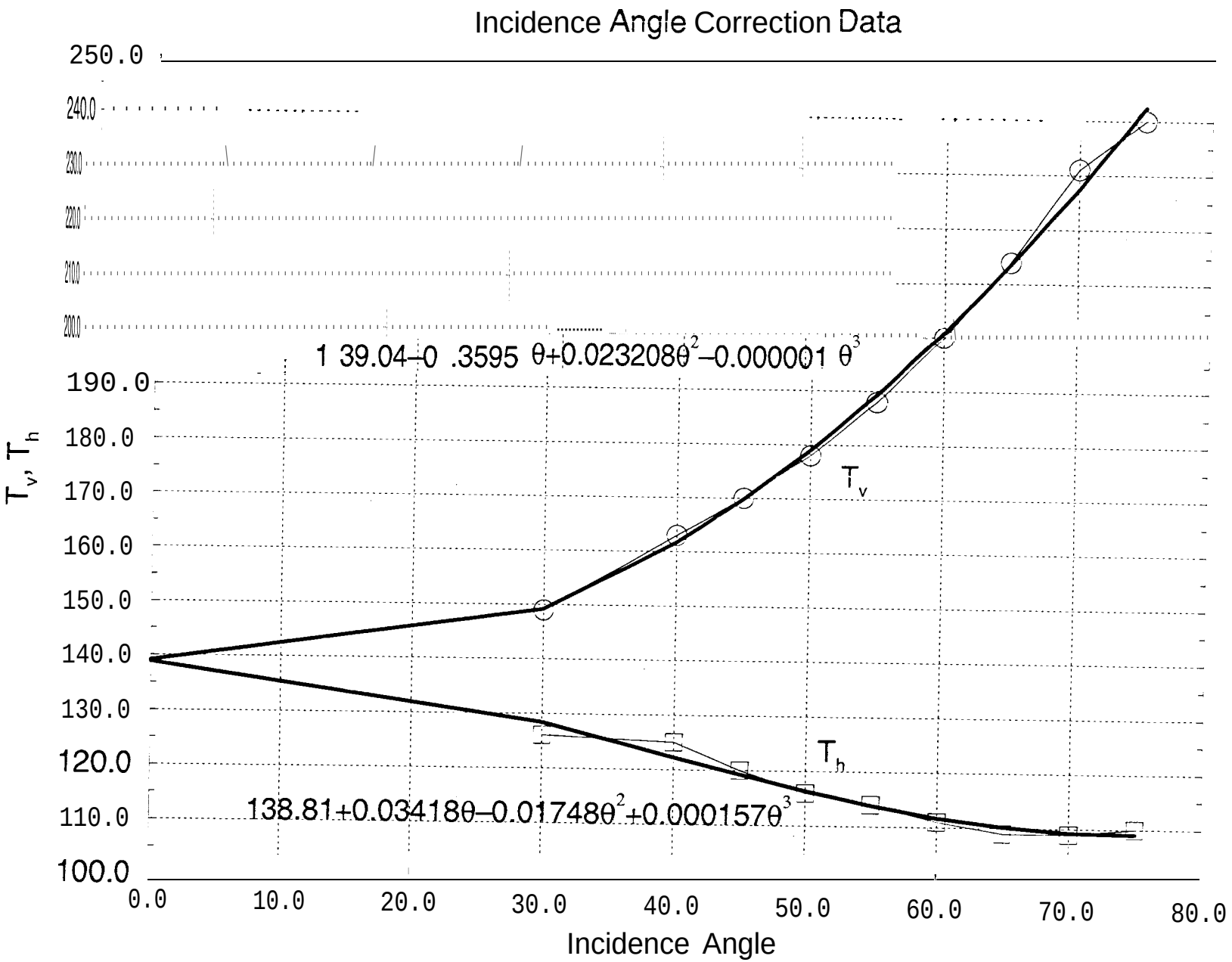
Incidence Angle Correction Data
250.0
240.0
230.0
220.0
210.0
200.0
190.0
180.0
170.0
160.0
150.0
140.0
130.0
120.0
110.0
100.0
T_v, T_h
1 39.04–0 .3595 θ+0.023208θ²–0.000001 θ³
T_v
T_h
138.81+0.034180–0.017480²+0.0001570³
0.0
10.0
20.0
30.0
40.0
50.0
60.0
70.0
80.0
Incidence Angle

JPL WINDRAD 11042044

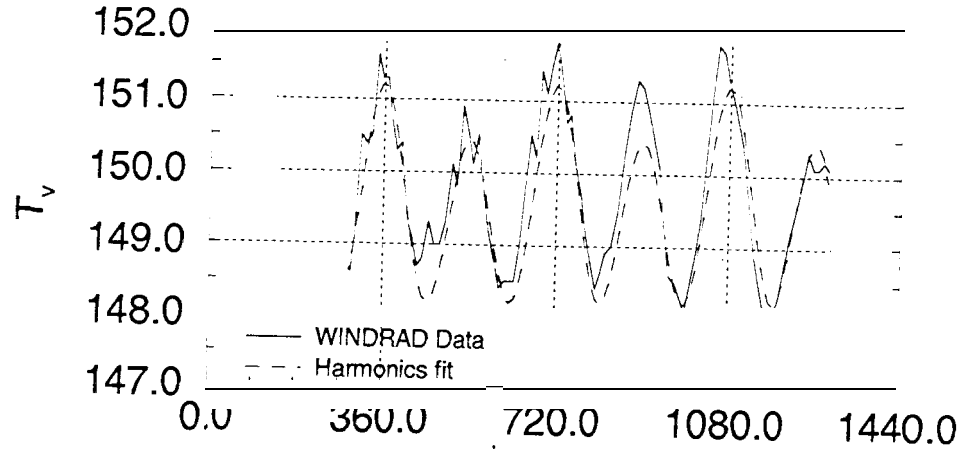

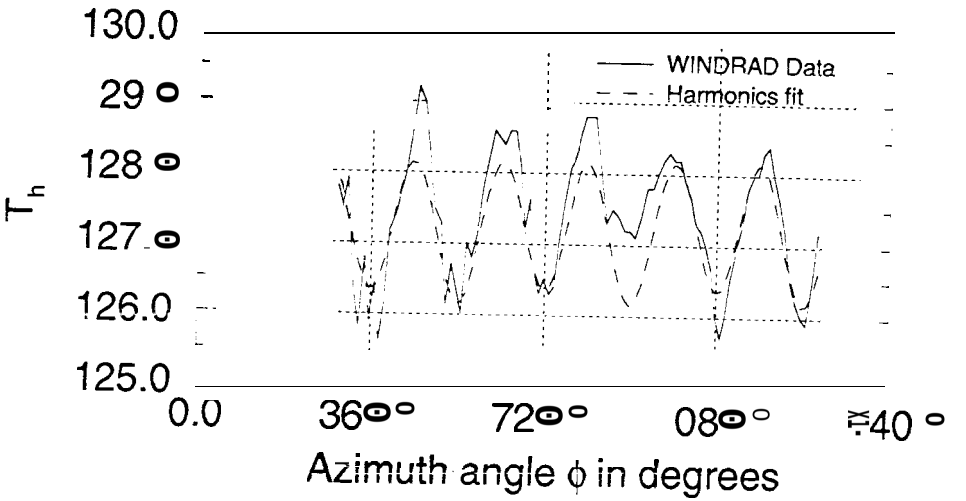

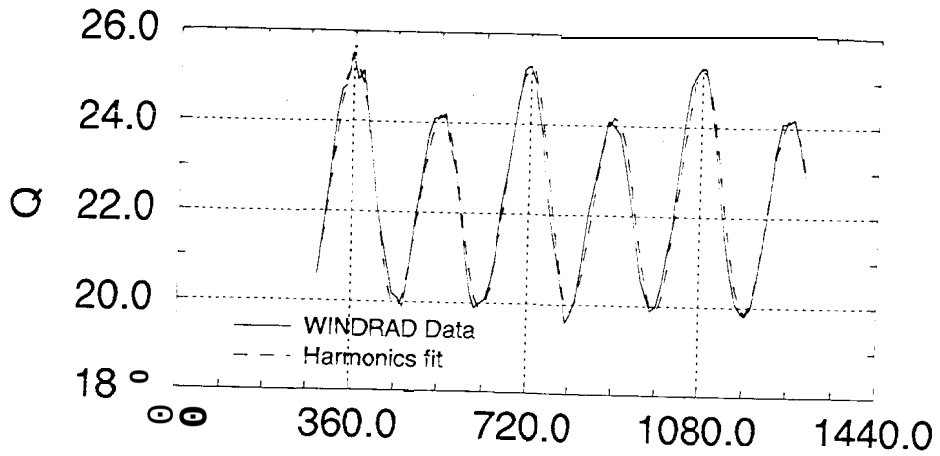

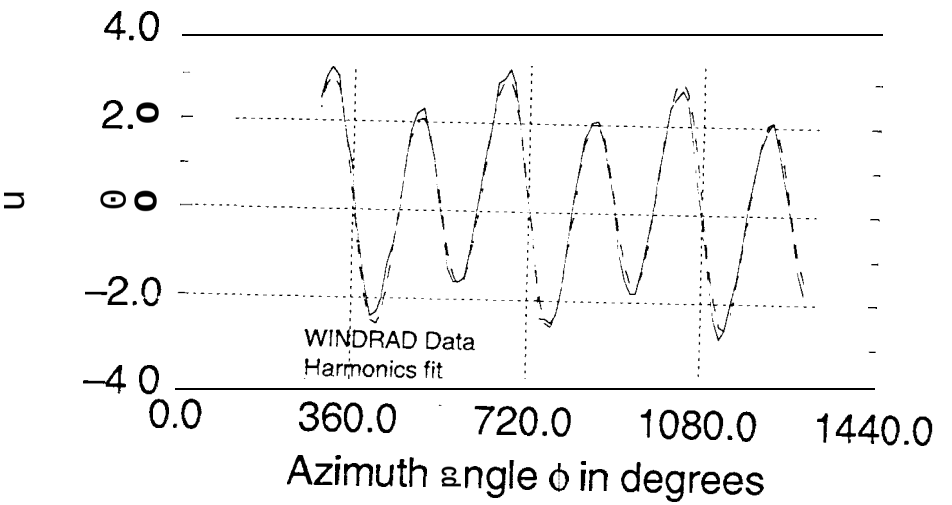

JPL WINDRAD 11–2038

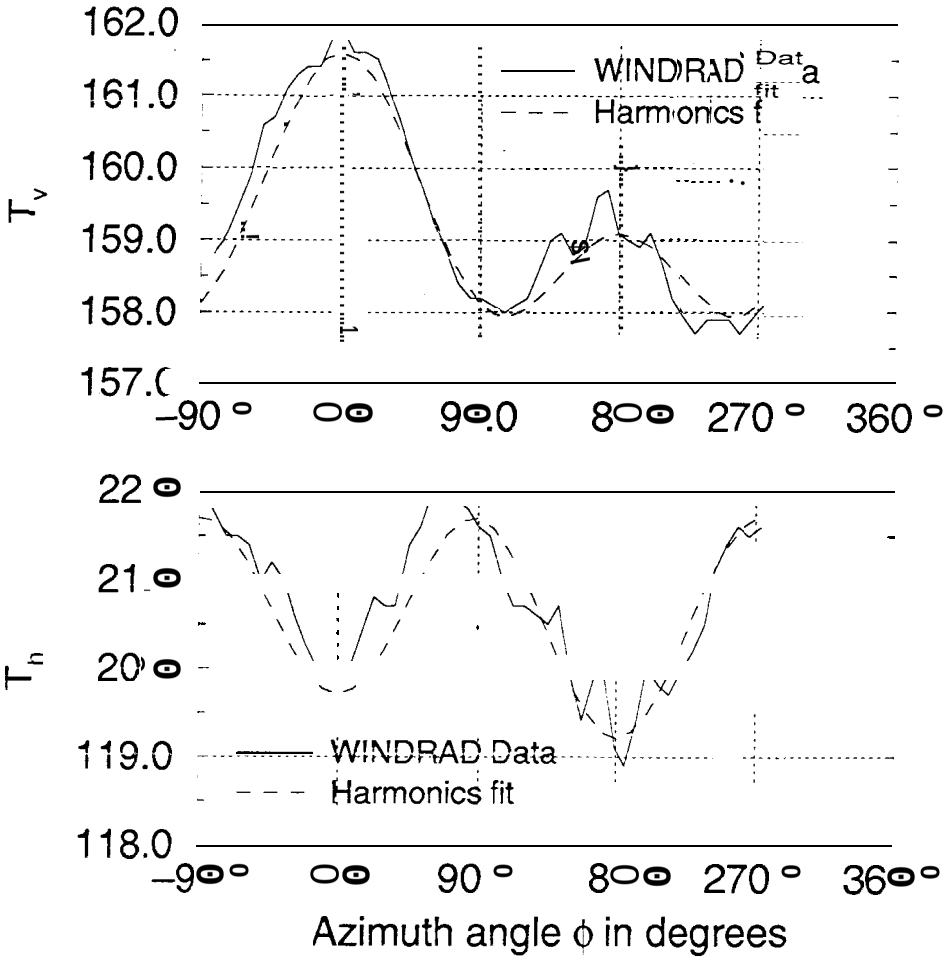

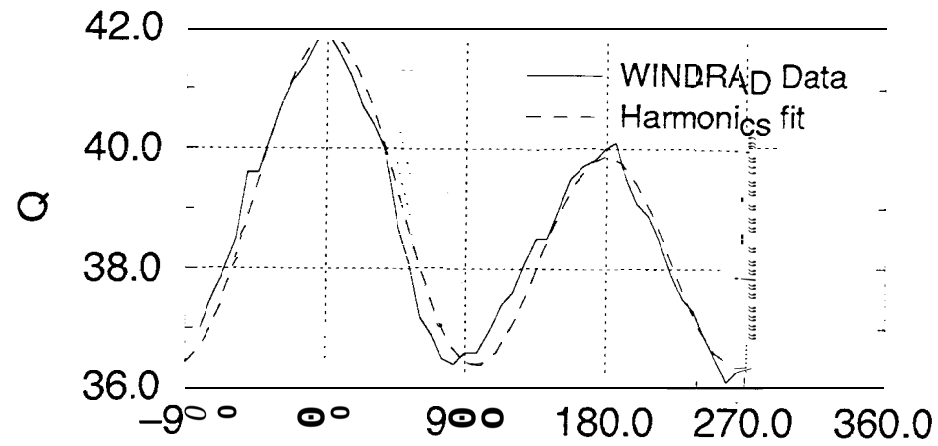

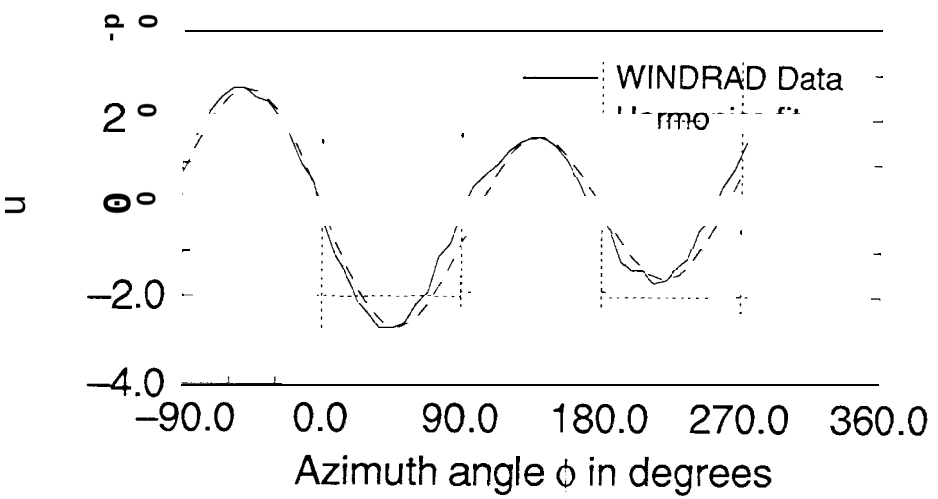

JPL WINDRAD 11042022

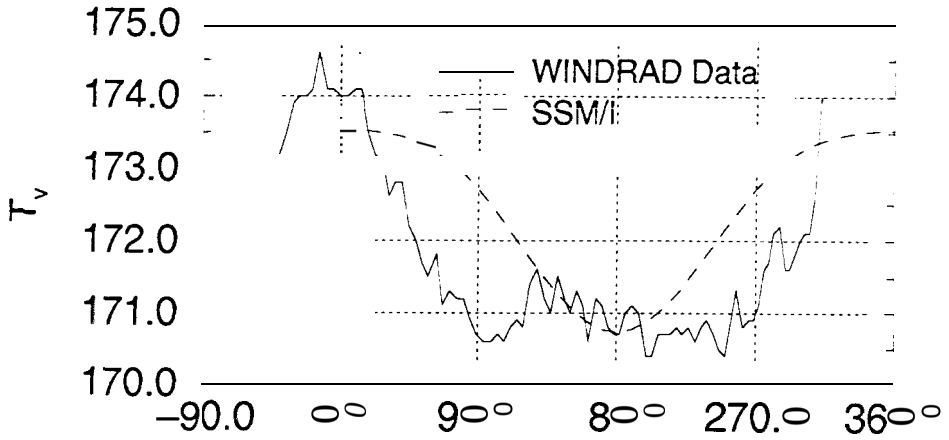

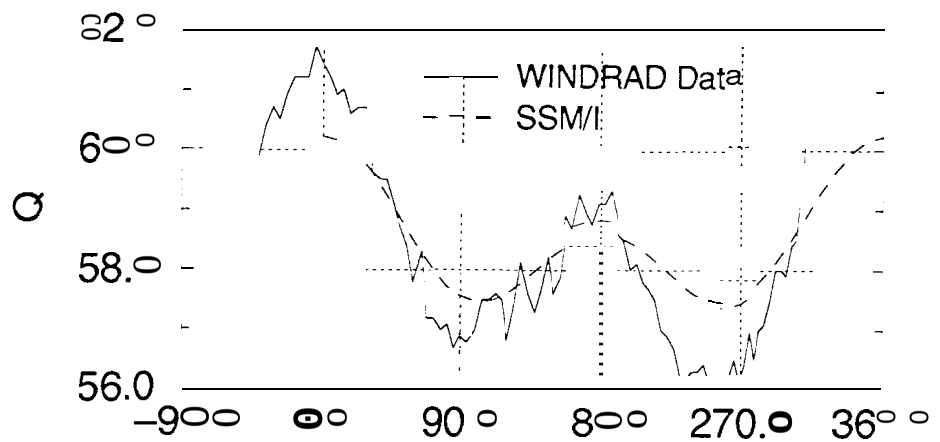

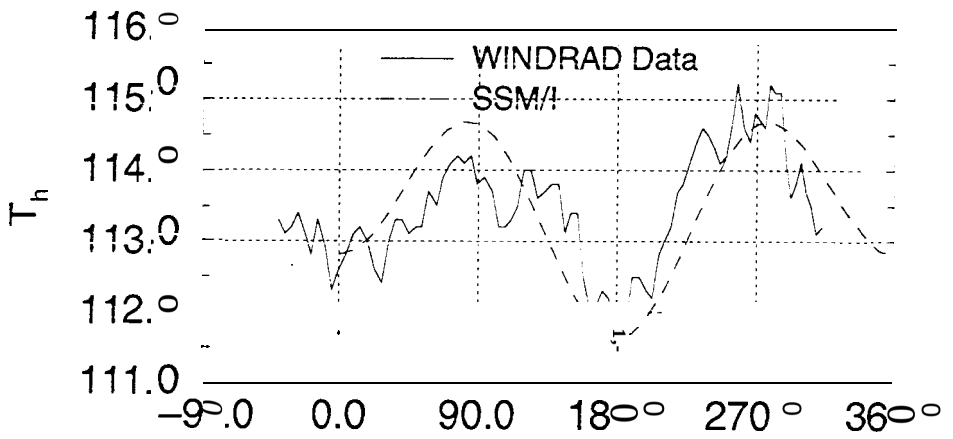

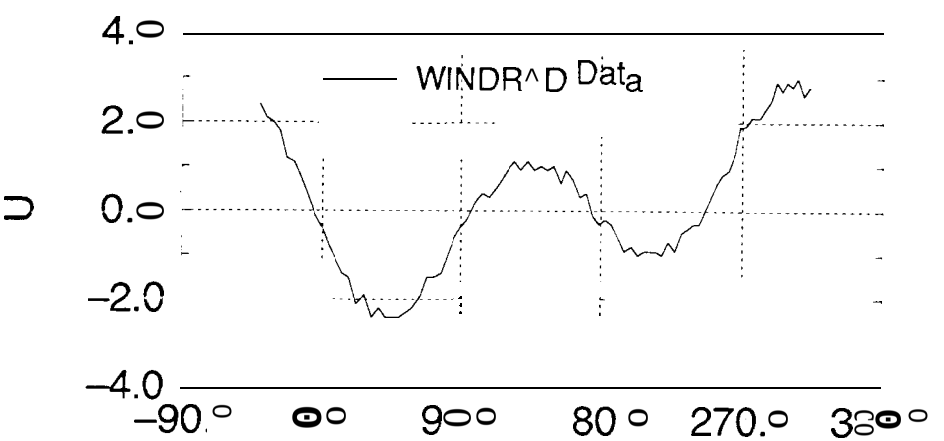

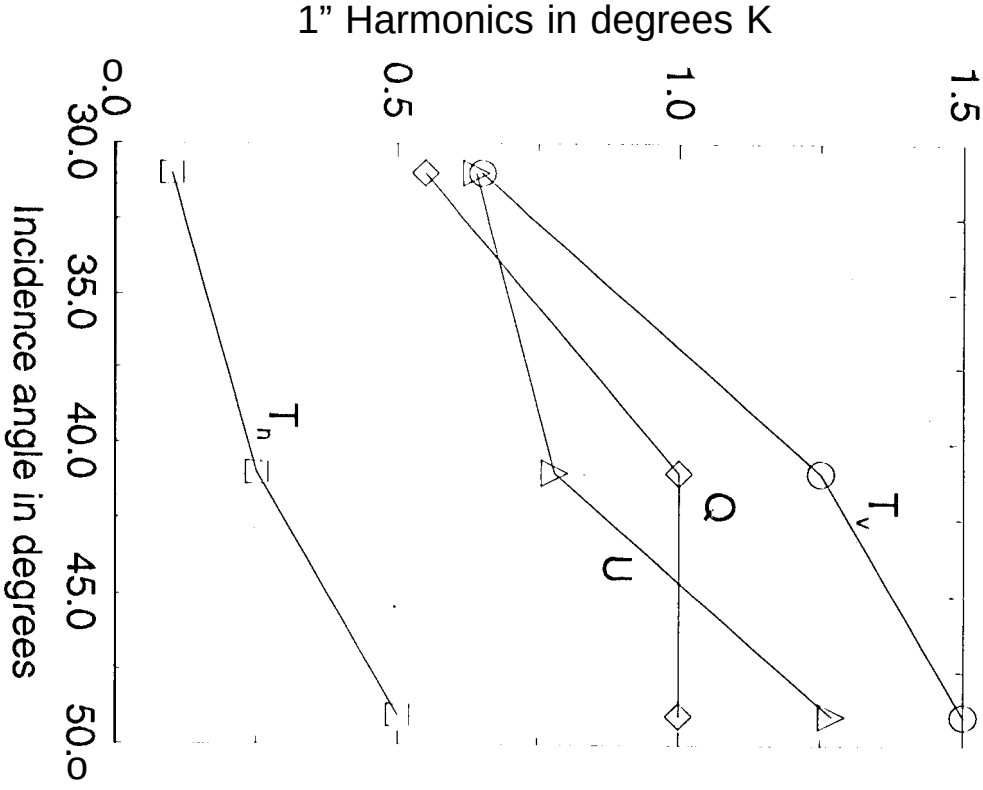
1” Harmonics in degrees K
0.0
0.5
1.0
1.5
30.0
35.0
40.0
45.0
50.0
Incidence angle in degrees
T_h
Q
U
T_v

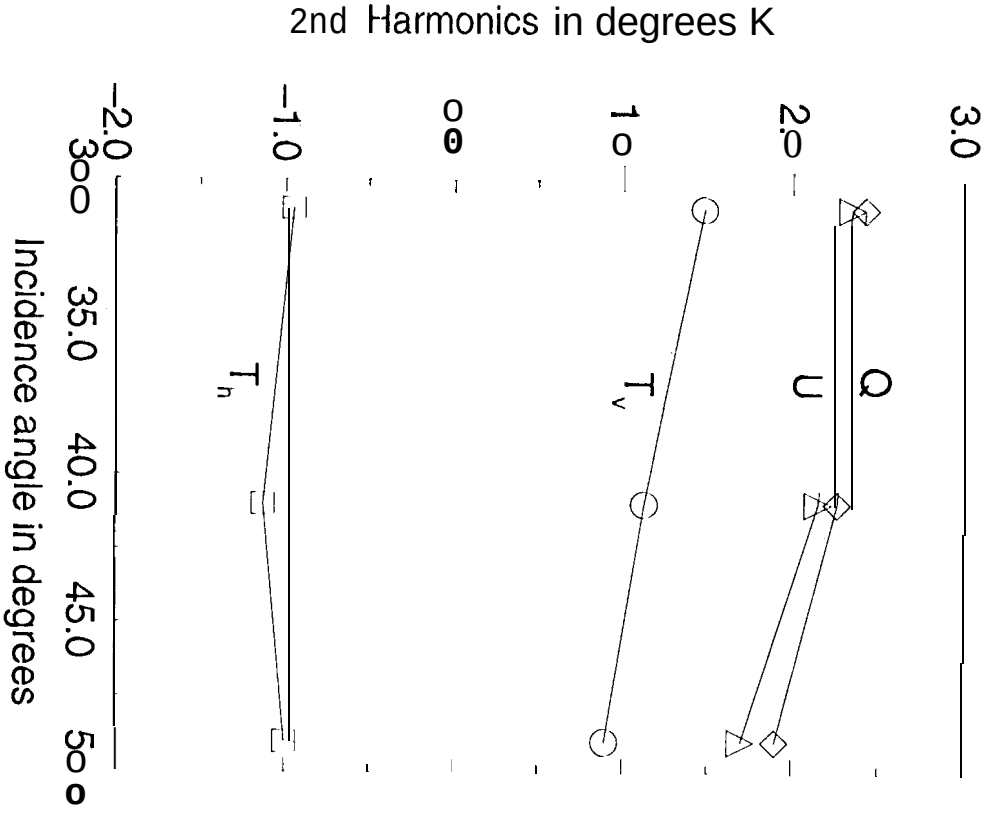
2nd Harmonics in degrees K
-2.0
-1.0
0.0
1.0
2.0
3.0
30.0
35.0
40.0
45.0
50.0
Incidence angle in degrees
T_h
T_v
U
Q

JPL WINDRAD 11172120

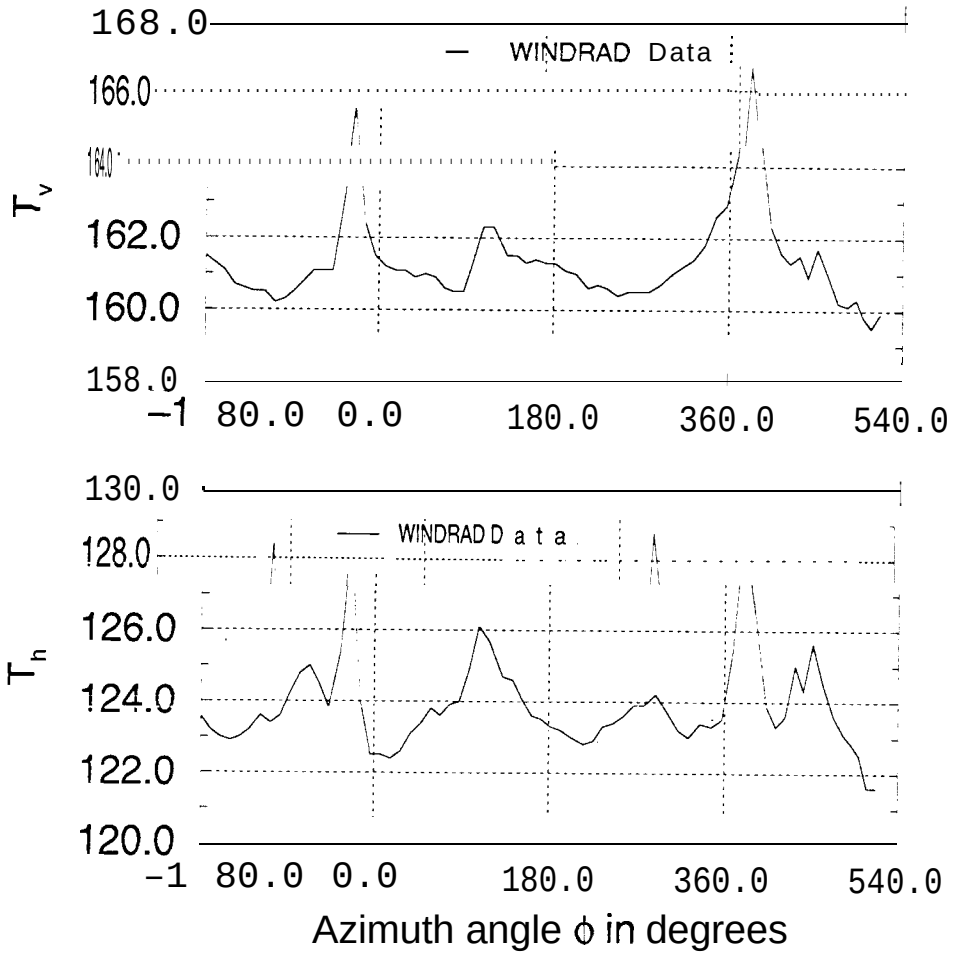

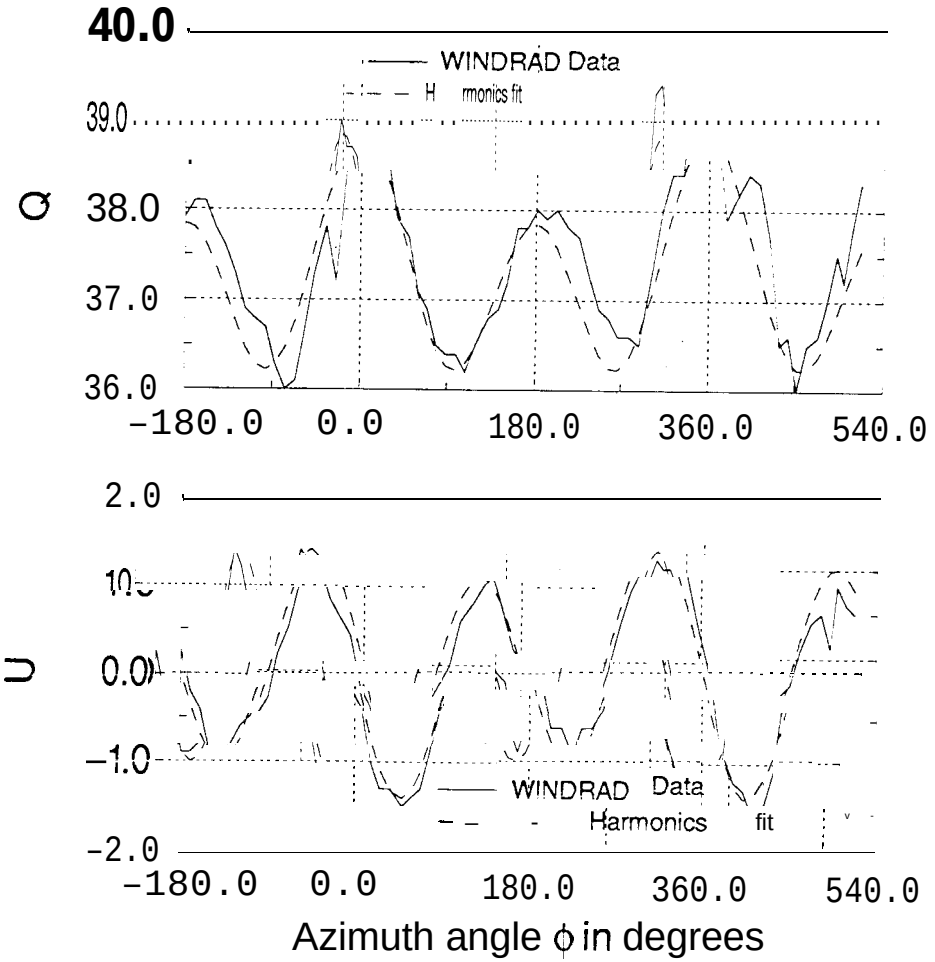

Fig. 8